Nonlocal response with local optics

Jiantao Kong, Alexander J. Shvonski, and Krzysztof Kempa*
Department of Physics, Boston College, Chestnut Hill, Massachusetts 02467, USA

(Received 8 December 2017; published 19 April 2018)

For plasmonic systems too small for classical, local simulations to be valid, but too large for *ab initio* calculations to be computationally feasible, we developed a practical approach—a nonlocal-to-local mapping that enables the use of a modified local system to obtain the response due to nonlocal effects to lowest order, at the cost of higher structural complexity. In this approach, the nonlocal surface region of a metallic structure is mapped onto a local dielectric film, mathematically preserving the nonlocality of the entire system. The most significant feature of this approach is its full compatibility with conventional, highly efficient finite difference time domain (FDTD) simulation codes. Our optimized choice of mapping is based on the Feibelman's d-function formalism, and it produces an effective dielectric function of the local film that obeys all required sum rules, as well as the Kramers-Kronig causality relations. We demonstrate the power of our approach combined with an FDTD scheme, in a series of comparisons with experiments and *ab initio* density functional theory calculations from the literature, for structures with dimensions from the subnanoscopic to microscopic range.

DOI: 10.1103/PhysRevB.97.165423

I. INTRODUCTION

Conventional numerical methods of studying plasmonic and nanophotonic systems, such as the finite difference time domain (FDTD) method [1], are based on solving Maxwell's equations on a grid of points in real space. At each grid point, two material parameters are defined: the electric permittivity ε and the magnetic permeability μ. In the most efficient and popular FDTD codes (MEEP, CST, and COMSOL) [2], these are functions of the propagating wave frequency (ω) only, and the important dependency on the wave vector q of the propagating wave is typically neglected. This is equivalent to the assumption of locality: The response of the medium at a point r in space is assumed to depend only on the material response at the same point r. However, nonlocal effects might become important, in particular, in the highly nonuniform regions of samples. Ways to treat them have been proposed, beginning with the pioneering work of Pekar [3], as well as in the follow-up works in the 1960′s [4] and the 1980′s [5], and more recently [6–11].

There is no easy way to include nonlocality in the FDTD numerical codes. The simplest is the phenomenological hydrodynamic model, which leads to a simple extension of the local Drude formula, with $\omega(\omega+i\gamma)$ replaced by $\omega(\omega+i\gamma)-\beta q^2$ [12]. The quantum mechanical d-function formalism of Feibelman [13] also provides a simple, analytical extension of local Fresnel optics (for small q). In addition to ε and μ, it introduces two surface dielectric response functions (d functions), which also depend only on ω [14]. Similar to ε and μ, these functions can be calculated in an *ab initio* manner for a given metal [15–17], and then used in simulating the response of metal-containing structures via a Fresnel-like strategy. However, while the d-function formalism was very useful in understanding the basic physics of surface plasmons on simple metallic surfaces and simple large-scale metallic structures, the treatment of more complex systems or ultrasmall nanostructures cannot benefit directly from this approach. As pointed out above, implementing this approach into highly efficient FDTD codes is difficult. In principle, nonlocality can be fully included in more fundamental treatments of the material equations, such as density functional theory (DFT) [18]. However, due to limitations on computer power, this *ab initio* approach can handle only ultrasmall structures, of hundreds of atoms at most (i.e., a few nm in diameter). Therefore, there is a need for a theory capable of handling nonlocal effects in nanostructures with intermediate sizes, at least for small q.

In an attempt to respond to this need, a recent work [19] proposed an idea of mapping the nonlocal surface region of a metal into a fictitious local dielectric effective film. The nonlocality of the surface region was modeled using the hydrodynamic approximation. This mapping was shown to be valid only for very small q and ω [20]. Recently, we employed a similar mapping, instead using the d-function formalism [21]. Both works produced mapping relations that were not unique and, therefore, additional constraints were needed. In Refs. [19–21] no effort was made to make the local dielectric functions of the fictitious films physical; these were just mapping functions. However, physicality (at least causality) of the dielectric functions is implied by the FDTD schemes. In this paper, we optimize the mapping process, and require that the resulting dielectric functions are physical, i.e., they satisfy all the conditions required, including causality and various sum rules. We show that our mapping works quantitatively in a much larger region of phase space (q-ω) than the earlier mapping [19,21]. We demonstrate that, with our mapping, the conventional FDTD simulations acquire nonlocal capability, sufficient for a quantitative description of various nanoscopic systems.

*Author to whom correspondence should be addressed: kempa@bc.edu

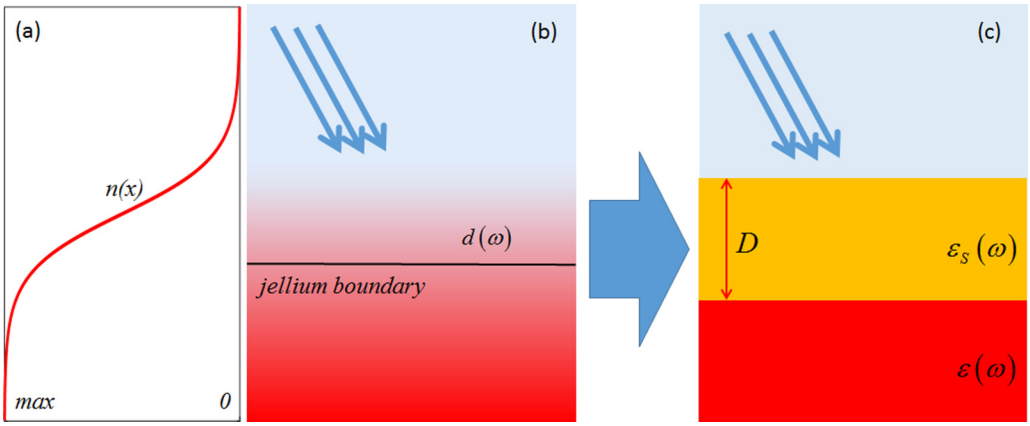

FIG. 1. (a) Diffusive character of electron density profile $n(x)$ at a metal surface. (b) Gradient of the red color represents the diffusive profile of electrons confined by the jellium (the uniform positive charge, extending below the jellium boundary). (c) Local model of the metal surface, with a hypothetical film (orange color) of thickness D replacing the nonuniform electron density profile in the transition region.

II. NONLOCAL-TO-LOCAL MAPPING

Consider an interface between a metal and vacuum where huge electron density gradients exist. While in the classical description, metal electrons are sharply confined to the bulk, quantum mechanics predicts the electron density near the metal surface to have a smooth profile $n(x)$, as shown schematically in Figs. 1(a) and 1(b). The transition region thickness is of order D. Such a smooth electron density profile can be calculated self-consistently in the jellium model [22]. The electromagnetic response for a metallic surface with such a profile has been calculated [15–17], and allowed the determination of the d functions for many metals. The d-function formalism provides closed formulas for long-wavelength, nonlocal extensions of local Fresnel formulas, thus, it is a perfect platform to develop a nonlocal-to-local mapping. In our earlier work [21] we based the mapping on the Feibelman formula [13] for the reflection coefficient of a p-polarized light. By comparing this expression to the corresponding small-D expansion of the local, Fresnel reflection coefficient for the model shown in Fig. 1(c), we obtained the effective dielectric function of the fictitious film [21],

$$\varepsilon_s(\omega) = \frac{D\varepsilon(\omega)}{[\varepsilon(\omega)-1]d(\omega)}, \tag{1}$$

where $\varepsilon(\omega)$ is the Drude dielectric function of the metal and $d(\omega)$ is the d function. Even though ε_s obtained from Eq. (1) follows from a correct, formal mapping procedure, it is unphysical. This is due to an *ad hoc* choice, $\varepsilon_s(\omega) \propto D$, employed in the derivation of Eq. (1). Clearly, ε_s diverges for large ω, since $\varepsilon(\omega) \to 1$, and $d(\omega) \propto \int_{-\infty}^{\infty} x\delta\rho(x)dx \to 0$ (the induced charge density $\delta\rho$ vanishes for sufficiently large frequency). Moreover, ε_s violates causality. To see this, we examine the corresponding susceptibility,

$$\chi_s(\omega) = \frac{\varepsilon_s(\omega)-1}{4\pi} = \frac{D[1+4\pi\chi(\omega)]}{4\pi\chi(\omega)d(\omega)}. \tag{2}$$

Causality requires that proper response functions (e.g., susceptibility), when analytically continued into the upper complex half plane of variable $z = \mathrm{Re}(\omega) + i\,\mathrm{Im}(\omega)$, are analytic and vanish for $|z| \to \infty$ and $\mathrm{Im}(\omega) > 0$ [23]. Since the Drude susceptibility $\chi(\omega)$ and $d(\omega)$ are causal, they satisfy these conditions, and so from Eq. (2) we have, for $|z| \to \infty$ and $\mathrm{Im}(\omega) > 0$,

$$\chi_s(z) = \frac{D[1+4\pi\chi(z)]}{4\pi\chi(z)d(z)} \to \infty. \tag{3}$$

This is a clear violation of the causality condition.

To eliminate this problem, we have investigated several alternative effective response functions within Feibelman's formalism, requiring that, in addition to the required nonlocal-to-local mapping, they lead to causal ε_s. We identified only one, physical ε_s, based on Liebsch's formula for the generalized reflection coefficient [24],

$$g(q,\omega) \approx \frac{\varepsilon(\omega)-1}{\varepsilon(\omega)+1-2q\varepsilon(\omega)d(\omega)}. \tag{4}$$

The local Fresnel reflection coefficient for the model structure shown in Fig. 1(c) is [25,26]

$$g(q,\omega) = \frac{\varepsilon'(q,\omega)-1}{\varepsilon'(q,\omega)+1}, \tag{5}$$

where

$$\varepsilon'(q,\omega) = \varepsilon_s(\omega)\frac{\varepsilon(\omega)+\varepsilon_s(\omega)+[\varepsilon(\omega)-\varepsilon_s(\omega)]e^{-2qD}}{\varepsilon(\omega)+\varepsilon_s(\omega)-[\varepsilon(\omega)-\varepsilon_s(\omega)]e^{-2qD}}. \tag{6}$$

It can be shown [27] that for $Dq \ll 1$, and with

$$\varepsilon_s(\omega) = \varepsilon(\omega)\left[1-\frac{d(\omega)}{D}\right], \tag{7}$$

Eq. (5) reduces to Eq. (4). Another derivation of this result is also provided in Ref. [27].

The effective dielectric function of the fictitious film, given by Eq. (7), is causal. The corresponding expression for the susceptibility is

$$\chi_s(\omega) = \frac{\varepsilon_s(\omega)-1}{4\pi} = \frac{1}{4\pi}\left\{[1+4\pi\chi(\omega)]\left[1-\frac{d(\omega)}{D}\right]-1\right\}. \tag{8}$$

Clearly, $\chi_s(\omega)$ vanishes for $|z| \to \infty$ and $\mathrm{Im}(\omega) > 0$. In addition, since $\chi(\omega)$ and $d(\omega)$ are causal, $\chi_s(\omega)$ also is analytic

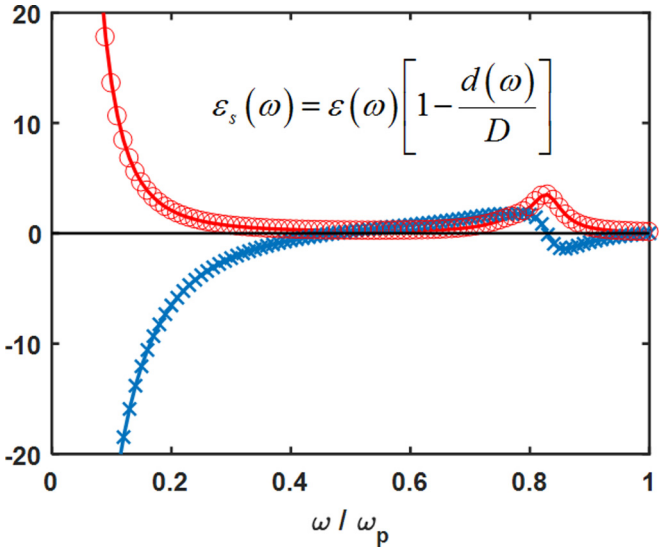

FIG. 2. Effective dielectric function ε_s of the fictitious film shown in Fig. 1(c), plotted vs ω/ω_p, for potassium as an example. The inset shows the analytical expression for ε_s, also listed as Eq. (7) in text. Solid lines represent the analytical evaluation of this equation: Re[ε_s] (blue) and Im[ε_s] (red). Symbols represent the corresponding numerical results based on Kramers-Kronig relations: Re[ε_s] (blue crosses) and Im[ε_s] (red circles). See text for details.

in the upper complex half plane of variable z. Thus, all the conditions for the causality of $\chi_s(\omega)$ are satisfied and Eq. (7) represents a causal (i.e., physical) dielectric function.

To further illustrate that causality is satisfied, we checked that the Kramers-Kronig (KK) relations are satisfied numerically [23]. These follow the causality condition and have the following form,

$$\mathrm{Re}[\varepsilon_s(\omega)] = 1 + \frac{2}{\pi}\mathrm{P}\int_0^\infty \mathrm{Im}[\varepsilon_s(\omega')]\frac{\omega'}{\omega'^2 - \omega^2}d\omega', \quad (9)$$

$$\mathrm{Im}[\varepsilon_s(\omega)] = -\frac{2}{\pi}\mathrm{P}\int_0^\infty \mathrm{Re}[\varepsilon_s(\omega')]\frac{\omega}{\omega'^2 - \omega^2}d\omega', \quad (10)$$

where the integrals are evaluated along the real frequency axis, and P indicates the principle value integral. To check Eq. (9), we used Eq. (7) first to calculate Im[$\varepsilon_s(\omega')$]. Then, we numerically evaluated the integral on the right-hand side for a given ω, and thus obtained the numerical values of Re[$\varepsilon_s(\omega)$]. Here, we used the following explicit expression for the Drude dielectric function, $\varepsilon(\omega) = 1 - \omega_p^2/\omega(\omega + i\gamma)$, with ω_p the plasma frequency for potassium, the phonon-impurity scattering rate set as $\gamma = 0.05\omega_p$, and $d(\omega)$ taken from Ref. [15] for potassium, and then fitted to a Lorentzian form

$$d(\omega) = \sum_{s=1}^{2} \frac{A_s}{\omega_s^2 - \omega(\omega + i\gamma_s)}, \quad (11)$$

where $A_1 = 0.367, A_2 = 0.078$, $\omega_1 = 0.829$, $\omega_2 = 0.774$, $\gamma_1 = 0.063$, and $\gamma_2 = 0.097$. The numerically obtained values of Re[$\varepsilon_s(\omega)$] can be compared with the exact values of Re[$\varepsilon_s(\omega)$], obtained directly from Eq. (7). Figure 2 shows that, as expected, the two values are essentially identical. The same procedure was used to check the second KK relation [Eq. (10)], confirming the validity of this condition as well. This confirms that the dielectric function given by Eq. (7) is causal. Equation (7) is the *main result* of this article.

In addition to satisfying KK relations, the dielectric function given by Eq. (7) has the characteristic Drude-like form with a reduced, effective plasma frequency $\bar{\omega}_p$, as expected for a metal film modeling the diffusive region, where the electron density is reduced. Also, we have checked numerically that the dielectric function satisfies the following sum rules [28],

$$\int_0^\infty \omega\mathrm{Im}[\varepsilon_s(\omega)]d\omega = \frac{\pi}{2}\bar{\omega}_p^2, \quad (12)$$

$$\int_0^\infty \omega\mathrm{Im}[\varepsilon_s(\omega)]^{-1}d\omega = -\frac{\pi}{2}\bar{\omega}_p^2, \quad (13)$$

$$\int_0^\infty \mathrm{Im}[\varepsilon_s(\omega)]^{-1}\frac{d\omega}{\omega} = -\frac{\pi}{2}. \quad (14)$$

While the last sum rule [Eq. (14)] is exactly and unconditionally satisfied, the first two [Eqs. (12) and (13)] yield an identical, reduced effective plasma frequency equal to $\bar{\omega}_p = 0.7448\omega_p$. This frequency is larger than the zero crossing of Re[$\varepsilon_s(\omega)$] in Fig. 2, which occurs at $\omega \approx 0.5\omega_p$. In interpreting this discrepancy, one should keep in mind that, while the sum rules are strictly valid only for a homogeneous electron gas, this is not the case in the surface region described by the fictitious film.

III. APPLICATIONS IN PLASMONIC SYSTEMS

To demonstrate the strength and robustness of the mapping based on Eq. (7), in the remaining part of this paper we apply it to a few prototypical plasmonic systems, and compare with data available in the literature. First, we study the plasmonic resonance of sodium spheres/particles, which is known to be redshifted from its classical prediction, with the Mie resonance given by $\omega_{\mathrm{Mie}} = \omega_p/\sqrt{3}$ [24]. In addition, this redshift increases with decreasing particle size. The Mie resonance is shown in Fig. 3(a) as the black solid line. The *ab initio* DFT calculation for the same system [29] yields black squares in Fig. 3(a)—a redshifted resonance. Implementing our effective film approach, i.e., coating the (classical) sphere with the film of a metal-like material having a dielectric function given by Eq. (7), and performing the conventional FDTD simulation, yields the colored lines in Fig. 3(a), in good agreement with the DFT result for a range of the film thickness. This insensitivity of our simulation outcome to the film thickness choice is an important feature, since the film thickness is an adjustable parameter, constrained loosely only by the size of the diffusive region at the metal surface.

In Fig. 3(b), we plot the normalized plasmon resonance frequencies for sodium spheres versus the inverse sphere radius. We compare here our effective film scheme (for three different film thicknesses) with experimental results and other theoretical studies reported in Ref. [30]. The results for the chosen film thickness of 0.3 nm agree best with those from experiments and advanced theories. This is consistent with the average thickness of the diffusive region D, as obtained from microscopic models [22], and shows that it can be used

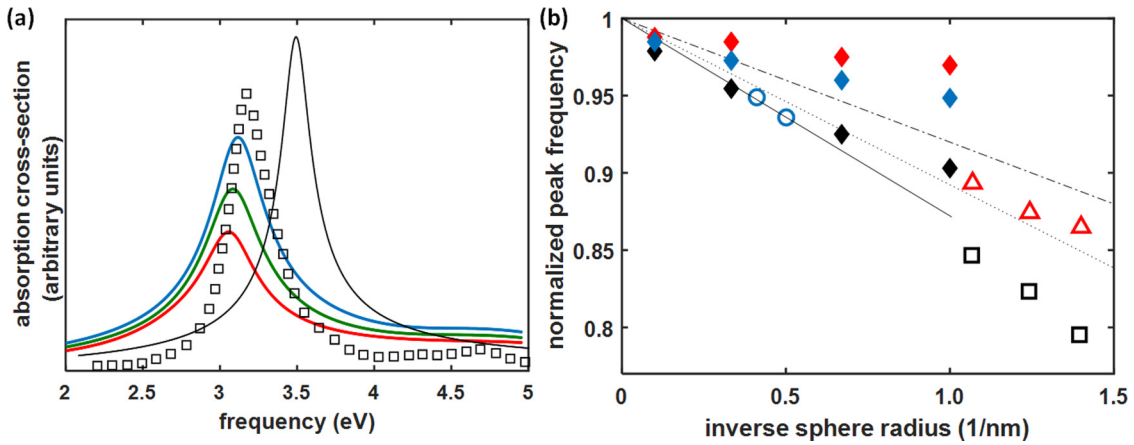

FIG. 3. (a) Plasmonic response spectrum (absorption cross section in arbitrary units) of a sodium sphere of radius 1.4 nm. Classical Mie resonance is shown as the black solid line. Open squares are *ab initio* DFT results adapted from Ref. [29]. Red/green/blue solid lines are from our effective film scheme with film thickness equal to 0.3, 0.4, and 0.5 nm respectively. (b) Normalized frequencies of plasmon resonances (peak positions) for sodium spheres vs the inverse sphere radius. Effective film approach results: Red/black/blue diamonds with the corresponding film thickness 0.1, 0.3, and 0.9 nm, respectively. Open circles, triangles, and squares are experimental data adapted from Ref. [30]. Solid, dotted, and dashed-dotted lines are advanced theoretical models discussed in Ref. [30].

as an appropriate choice of the fictitious film thickness. The negative slope of the curve in Fig. 3(b) is identical to the characteristic negative slope of surface plasmons on a planar sodium surface. This is a universal property for all alkali metals [31]; a one-to-one correlation between the slopes is facilitated by the simple surface plasmon "whispering gallery" relation $2\pi R = \lambda$ [32], which reduces to $q \approx 1/R$.

In the last test of our scheme, we applied it to a previously studied case of the electric field enhancement in between two closely spaced sodium spheres, tuned out of the plasmonic (Mie) resonance. Each sphere has diameter $2R = 2.8$ nm, and thickness of the surface region (shown gray in the insets) $d = 0.35$ nm. The frequency of the driving field is $\hbar\omega = 2.75$ eV. Figure 4 shows the electric field enhancement halfway between the two sodium spheres versus the intersphere gap size. Our scheme results are shown as red diamonds. The blue circles represent calculations based on the hydrodynamic approximation (HDA) taken from Ref. [8]. These are valid only for gap sizes much greater than the width of the surface regions. The black circles represent *ab initio* DFT calculations taken from Ref. [29], which, due to numerical difficulties, are possible only for ultrasmall spheres and gaps. Thus, *only our results* span the small to large gap sizes.

Our results show a sharp decrease in the field enhancement for gap sizes less than $2d$. This steplike decrease is physical, and is the result of the presence of a surface region (of thickness $\sim d$) of reduced electron density, at metallic surfaces. As long as the two spheres are farther than $2d$ apart, the midpoint (where field is calculated) lies in vacuum, and thus the electric field is only remotely (weakly) screened by the polarized spheres. However, once the surface regions begin to overlap for gap sizes $<2d$, the midpoint probes this overlap region of (on average) high electron density, and thus a very strong shielding takes place. In our simulations, as discussed above, the surface region is represented by a constant, reduced electron density, steplike region (marked gray in the insets). Consequently, the steplike discontinuity of the electric field enhancement at gap size of $2d$ is a result of this steplike model of the electron density. In more realistic calculations, in which the gradual surface electron density can be accommodated, a more gradual (but still quite sharp) transition of the field enhancement is expected. The most important conclusion here is that our simulations, valid everywhere, agree (to within an order of magnitude) with the available calculation results from the literature (DFT and HDA), in their respective regions of validity.

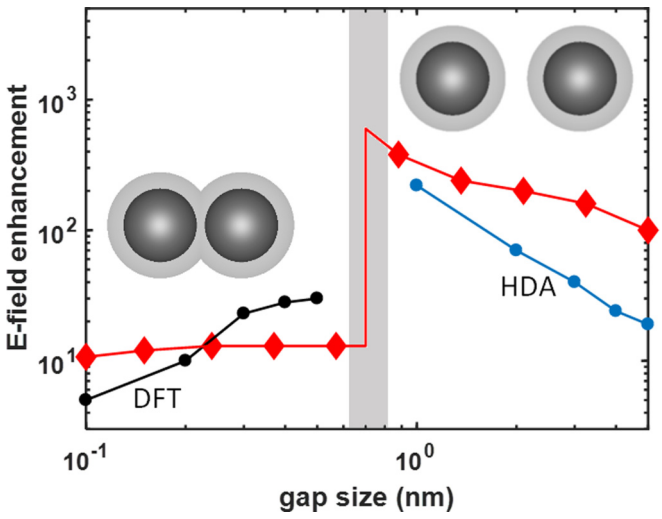

FIG. 4. Electric field enhancement halfway between two sodium spheres vs the intersphere gap. Each sphere has diameter $2R = 2.8$ nm, and thickness of the surface region (shown gray in the insets) $d = 0.35$ nm. The frequency of the driving field is $\hbar\omega = 2.75$ eV. Red diamonds represent our simulations, based on the effective (fictitious) film scheme. Black circles represent the *ab initio* DFT calculations [29], available only in the quantum regime. Blue circles show results of the hydrodynamic approximation [8], valid only in the classical regime. The insets show sketches of the spheres at an overlap (left) and well-spaced (right) cases, with diffusive regions marked gray.

IV. CONCLUSION

In conclusion, we propose an effective film approach for plasmonic and nanophotonic studies, which accounts for nonlocal effects caused by the nonuniform region at metal surfaces. The approach requires adding a fictitious, but physical, thin film with a specified dielectric response. In our scheme, this dielectric function is related to the d function. Adapted into classical FDTD calculation schemes, this approach produces a moderate q extension of all nonlocal response characteristics while avoiding the burdensome computations that are usually required by DFT for intermediate-size nanostructures. Specifically, we demonstrated that our method produces a quantitatively correct resonance shift and qualitatively correct field enhancement for small sodium spheres. While these examples have primarily focused on plasmonic systems with highly symmetric (e.g., spherical) geometries, we stress that our effective film approach may be applied to structures of any shape—the method simply requires coating all metal surfaces with a properly calculated thin film, and then performing the usual local FDTD simulation. Thus, our effective film method extends local FDTD calculations to a moderate q nonlocal regime. Our scheme suggests further improvements, for example, by increasing the number of fictitious films.

[1] A. Taflove and S. C. Hagness, *Computational Electrodynamics: The Finite-Difference Time-Domain Method* (Artech, Norwood, MA, 1995).

[2] MIT Electromagnetic Equation Propagation, Massachusetts Institute of Technology, http://ab-initio.mit.edu/wiki/index.php/Meep; CST Microwave Studio, the Computer Simulation Technology AG, https://www.cst.com/products/cstmws; COMSOL Multiphysics Modeling Software, https://www.comsol.com/

[3] S. I. Pekar, Theory of electromagnetic waves in a crystal with excitons, J. Phys. Chem. Solids **5**, 11 (1958).

[4] J. J. Hopfield and D. G. Thomas, Theoretical and experimental effects of spatial dispersion on the optical properties of crystals, Phys. Rev. **132**, 563 (1963).

[5] V. M. Agranovich and V. L. Ginzburg, *Crystal Optics with Spatial Dispersion, and Excitons* (Springer, Berlin, 1984).

[6] N. A. Mortensen, S. Raza, M. Wubs, T. Sondergaard, and S. I. Bozhevolnyi, A generalized non-local optical response theory for plasmonic nanostructures, Nat. Commun. **5**, 3809 (2014).

[7] T. V. Teperik, P. Nordlander, J. Aizpurua, and A. G. Borisov, Robust Subnanometric Plasmon Ruler by Rescaling of the Nonlocal Optical Response, Phys. Rev. Lett. **110**, 263901 (2013).

[8] C. Ciraci, R. T. Hill, J. J. Mock, Y. Urzhumov, A. I. Fernandez-Dominguez, S. A. Maier, J. B. Pendry, A. Chilkoti, and D. R. Smith, Probing the ultimate limits of plasmonic enhancement, Science **337**, 1072 (2012).

[9] F. J. Garcia de Abajo, Nonlocal effects in the plasmons of strongly interacting nanoparticles, dimers, and waveguides, J. Phys. Chem. C **112**, 17983 (2008).

[10] Y. Luo, R. Zhao, and J. B. Pendry, van der Waals interactions at the nanoscale: The effects of nonlocality, Proc. Natl. Acad. Sci. USA **111**, 18422 (2014).

[11] J. M. McMahon, S. K. Gray, and G. C. Schatz, Nonlocal Optical Response of Metal Nanostructures with Arbitrary Shape, Phys. Rev. Lett. **103**, 097403 (2009).

[12] F. Forstmann and R. Gerhardts, *Metal Optics Near the Plasma Frequency*, Springer Tracts in Modern Physics Vol. 109 (Springer, Berlin, 1986).

[13] P. J. Feibelman, Surface electromagnetic fields, Prog. Surf. Sci **12**, 287 (1982).

[14] For jellium metals, one of the d functions can be made to vanish by choosing the origin at the jellium edge.

[15] A. Liebsch, Dynamical screening at simple-metal surfaces, Phys. Rev. B **36**, 7378 (1987).

[16] K. Kempa and W. L. Schaich, Calculation of corrections to Fresnel optics from density response, Phys. Rev. B **34**, 547 (1986).

[17] P. Apell, A. Ljungbert, and S. Lundqvist, Non-local optical effects at metal surfaces, Phys. Scr. **30**, 367 (1984).

[18] W. Kohn and L. J. Sham, Self-consistent equations including exchange and correlation effects, Phys. Rev. **140**, A1133 (1965).

[19] Y. Luo, A. I. Fernandez-Dominguez, A. Wiener, S. A. Maier, and J. B. Pendry, Surface Plasmons and Nonlocality: A Simple Model, Phys. Rev. Lett. **111**, 093901 (2013).

[20] W. L. Schaich, Comment on Surface Plasmons and Nonlocality: A Simple Model, Phys. Rev. Lett. **115**, 239401 (2015).

[21] A. J. Shvonski, J. Kong, and K. Kempa, Nonlocal extensions of the electromagnetic response of plasmonic and metamaterial structures, Phys. Rev. B **95**, 045149 (2017).

[22] N. D. Lang and W. Kohn, Theory of metal surfaces: Charge density and surface energy, Phys. Rev. B **1**, 4555 (1970).

[23] F. W. Byron and R. W. Fuller, *Mathematics of Classical and Quantum Physics* (Dover, New York, 1992).

[24] A. Liebsch, *Electronic Excitations at Metal Surfaces* (Springer, New York, 1997).

[25] E. A. Stern and R. A. Ferrel, Surface plasma oscillations of a degenerate electron gas, Phys. Rev. **120**, 130 (1960).

[26] J. W. Gadzuk, Coupled surface-plasmon modes in metal-thin-film-vacuum sandwiches, Phys. Rev. B **1**, 1267 (1970).

[27] See Supplemental Material at http://link.aps.org/supplemental/10.1103/PhysRevB.97.165423 for details of derivation of Eq. (7).

[28] G. D. Mahan, *Many-Particle Physics* (Plenum, New York, 1990).

[29] P. Zhang, J. Feist, A. Rubio, P. Garcia-Gonzalez, and F. J. Garcia-Vidal, *Ab initio* nanophotonics: The impact of atomic structure, Phys. Rev. B **90**, 161407(R) (2014).

[30] T. Reiners, C. Ellert, M. Schmidt, and H. Haberland, Size Dependence of the Optical Response of Spherical Sodium Clusters, Phys. Rev. Lett. **74**, 1558 (1995).

[31] K.-D. Tsuei, E. W. Plummer, and P. J. Feibelman, Surface-Plasmon Dispersion in Simple Metals, Phys. Rev. Lett. **63**, 2256 (1989).

[32] Y. Wang, E. W. Plummer, and K. Kempa, Foundation of plasmonics, Adv. Phys. **60**, 799 (2011).